MEDICAL SCIENCE MONITOR

ANIMAL STUDY

e-ISSN 1643-3750
© Med Sci Monit, 2020; 26: e926187
DOI: 10.12659/MSM.926187

Received: 2020.05.21
Accepted: 2020.08.26
Available online: 2020.09.23
Published: 2020.11.18

Altered Inflammatory Pathway but Unaffected Liver Fibrosis in Mouse Models of Nonalcoholic Steatohepatitis Involving Interleukin-1 Receptor-Associated Kinase 1 Knockout

Authors' Contribution:
Study Design A
Data Collection B
Statistical Analysis C
Data Interpretation D
Manuscript Preparation E
Literature Search F
Funds Collection G

BCDE Ying Lei*
BEFG Tianxiao Yang*
CDG Aijing Shan
BC Wei Di
EFG Mengyao Dai
B Jingminjie Nan
B Dongxue Liu
AEG Yanan Cao
AEG Xiuli Jiang

Department of Endocrine and Metabolic Diseases, Shanghai Institute of Endocrine and Metabolic Diseases, National Clinical Research Centre for Metabolic Diseases, Key Laboratory for Endocrine and Metabolic Diseases of the National Health Commission, Shanghai Key Laboratory for Endocrine Tumors, Ruijin Hospital, Shanghai Jiao Tong University School of Medicine, Shanghai, P.R. China

* Ying Lei and Tianxiao Yang contributed equally to this work

Corresponding Author: Xiuli Jiang, e-mail: xiulijiang@126.com

Source of support: This work is supported by the National Natural Science Foundation of China (Grant No. 81522032, No. 81670793, No. 81870528, No. 81700681 and No. 81701458); National Key Research and Development Program (Grant No. 2016YFC0905001 and No. 2017YFC0909703); Shanghai Municipal Education Commission-Gaofeng Clinical Medicine Grant (Grant No. 20171905); National Natural Science Foundation of China (Grant No. 81701458); China Postdoctoral Science Foundation (Grant No. 2019M661563) and Institute of Shanghai Municipal Commission of Health and Family Planning (Grant No. 20174Y0219)

Background: Interleukin-1 receptor-associated kinases (IRAKs) are crucial mediators in the signaling pathways of Toll-like receptors (TLRs)/IL1Rs. Targeting the IRAK4/IRAK1/TRAF6 axis and its associated pathway has therapeutic benefits in liver fibrosis. However, the function of IRAK1 itself in the development of liver fibrosis remains unknown.

Material/Methods: *Irak1* global knockout (KO) mice were generated to study the functional role of *Irak1* in liver fibrosis. Male *Irak1* knockout and control mice were challenged with chronic carbon tetrachloride (CCl_4) or fed a methionine- and choline-deficient diet (MCDD) to generate models of nonalcoholic steatohepatitis (NASH). Liver inflammation and collagen deposition were assessed by histological examination, quantitative real-time PCR (qRT-PCR), and western blotting of hepatic tissues.

Results: The mRNA expression of the downstream inflammatory gene *Il1*β was significantly lower in *Irak1*-KO than in control mice. *Irak1* ablation had little effect on inflammatory cell infiltration into livers of mice with NASH. Collagen deposition and the expression of genes related to fibrogenesis were similar in the livers of *Irak1*-KO and control mice exposed to CCl_4 and MCDD. The loss of *Irak1* did not affect lipid or glucose metabolism in these experimental models of steatohepatitis.

Conclusions: *Irak1* knockout reduced the expression of inflammatory genes but had no effect on hepatic fibrogenesis. The *Irak1*-related pathway may regulate liver fibrosis via other pathways or be compensated for by other factors.

MeSH Keywords: Carbon Tetrachloride Poisoning • Inflammation • Interleukin-1 Receptor-Associated Kinases • Liver Cirrhosis

Full-text PDF: https://www.medscimonit.com/abstract/index/idArt/926187

2600 — 9 30

Indexed in: [Current Contents/Clinical Medicine] [SCI Expanded] [ISI Alerting System] [ISI Journals Master List] [Index Medicus/MEDLINE] [EMBASE/Excerpta Medica] [Chemical Abstracts/CAS]

Background

Liver fibrosis is thought to result from a chronic wound healing response to continuous hepatocellular injury, which results in an inflammatory response and the subsequent activation of hepatic stellate cells (HSCs) [1–3]. HSCs express smooth muscle actin (α-SMA) and produce an excess of extracellular matrix proteins. HSCs are activated by the inflammatory activity of liver immunocytes [4]. The inflammatory response during chronic liver injury is a dynamic process, characterized by the intrahepatic accumulation of various types of immune cells, including macrophages. During the course of development of nonalcoholic steatohepatitis (NASH), these cells produce and release cytokines and inflammatory mediators, such as tumor necrosis factor (TNF), interleukin 1β (IL1β), and IL6 [5]. Toll-like receptors (TLRs) are pattern recognition receptors that are expressed by cells of the innate immune system and by parenchymal cells in the liver. Following activation by their respective ligands, TLRs recruit various adapter proteins to initiate intracellular pro-inflammatory/anti-inflammatory signaling cascades [6]. Inflammation induced by TLR4 can activate the IRAK4/IRAK1/TRAF6 axis, inducing the secretion of downstream profibrotic cytokines [7].

Interleukin-1 receptor (IL1R)-associated kinases (IRAKs) are key mediators in the TLR/IL1R signaling pathways [8]. The IRAK family consists of 4 members, IRAK1, IRAK2, IRAK-M (also known as IRAK3), and IRAK4. IRAK1 was the first member of the IRAKs to be discovered [6,9,10]. Following the stimulation of TLR/IL1R, MyD88 is recruited to the cytoplasmic Toll/IL1R (TIR) domain, which promotes the binding of IRAK4 to the receptor complex. The combination of MyD88 and IRAK4 can induce IRAK4-mediated phosphorylation, followed by the activation of IRAK1. IRAK1 subsequently interacts with TNF receptor-associated factor 6 (TRAF6) and either activates AP1 or forms the TAK1/TAB complex. The activation of mitogen-activated protein kinase (MAPK) can activate AP1. Activation of the TAK1/TAB complex induces the degradation of IκB, which activates NF-κB and helps coordinate with immune responses [6,11]. Hepatic fibrosis was shown to be attenuated in Myd88-deficient mice [12], and IRAK1 ablation was reported to attenuate IL1β/IRAK1 inflammatory signaling and further diminish polymicrobial sepsis and the progression of hepatocellular carcinoma (HCC) [13,14].

The IRAK1-associated TLR/IL1R pathway was found to relieve fibrosis following liver injury. Some microRNAs and inhibitors targeting this pathway, including miR-146a-5p and pacritinib [15–18], had beneficial effect on liver fibrosis. However, these microRNAs and inhibitors are multi-targeted, and the functions of IRAK1 itself in liver fibrogenesis have never been investigated. The present study was designed to assess the effects of *Irak1* on hepatic inflammation and fibrosis in mouse models of NASH. *Irak1* global knockout (KO) mice were generated, and these *Irak1* KO and control mice were chronically treated with carbon tetrachloride (CCl_4) or fed a methionine- and choline-deficient diet (MCDD) to generate mouse models of NASH.

Material and Methods

Animals and induction of NASH

All animal experiments conformed to the Guide for the Care and Use of Laboratory Animals issued by the United States National Institutes of Health. All protocols were approved by the Animal Care and Use Committee of Shanghai Jiao Tong University School of Medicine. Using CRISPR/Cas-mediated genome engineering, Cas9 and gRNA were co-injected into fertilized eggs of C57BL/6 mice to generate *Irak1* KO mice on a C57BL/6 background. The mice were genotyped using the primers
5'-GTCCACATATAGCTCTTGAGGAATG-3',
5'-TTCACTGCATTCTAGTTGTG-3',
5'-CAGTGAATAAGGCAATGGGCTGC-3', and
5'-CAGGGCACTTCGCTTGCTAAG-3'.
All mice were maintained under temperature-controlled conditions with a 12-h light/dark cycle and free access to drinking water and food. At age 8–10 weeks *Irak1* KO and control mice were randomly divided into 2 groups. In the first group, *Irak1* KO and control mice were intraperitoneally (i.p.) administered 0.5 ml·kg–1 CCl_4 (Aladdin, China, C112044) or vehicle (Aladdin, China, C116023) twice per week for 8 weeks. In the second group, the *Irak1* KO and control mice were fed an MCDD (Research Diets, USA, A02082002B) or a control diet (Research Diets, USA, A02082003B) for 6 weeks. The control diet contained 3 g L-methionine and 2 g choline bitartrate, whereas the MCDD contained no L-methionine or choline bitartrate. All mice were allowed free access to water throughout. The tissues were harvested 3 days after the last treatment, the mice were fasted for 12 hours and sacrificed, and tissue samples were harvested. Unless otherwise stated, all mice used for these experiments were male.

Histological analysis of liver

Dissected hepatic tissues were fixed, dehydrated, and embedded in paraffin according to standard procedures. The paraffin-embedded tissue samples were sliced into 5-μm thick sections, which were stained with hematoxylin and eosin (H&E) to assess liver morphology. Sections were also stained with Sirius red and Masson stain to assess collagen deposition. Areas positive for Sirius red and Masson stain were quantified by digital image analysis. Tissue samples were also immunohistochemically stained with antibodies to CD45 (Abcam, UK, AB10558) and F4/80 (Santa Cruz Biotechnology, USA, SC-377009) as

Indexed in: [Current Contents/Clinical Medicine] [SCI Expanded] [ISI Alerting System] [ISI Journals Master List] [Index Medicus/MEDLINE] [EMBASE/Excerpta Medica] [Chemical Abstracts/CAS]

markers for immunocytes and macrophages, respectively, according to standard protocols. Digital images were acquired by an Olympus microscope system and quantified by Photoshop.

Biochemical analysis

Concentrations of triglycerides (TG) (Kehua, China, 113), total cholesterol (TC) (Kehua, China, 130-1), alanine aminotransferase (ALT) (Nanjing Jiancheng, China, C009-2-1), and aspartate aminotransferase (AST) (Nanjing Jiancheng, China, C0010-2-1) in serum and liver tissue were measured using commercial kits, according to the manufacturers' instructions. Glucose concentrations in tail blood were measured with One-Touch Ultra glucometers (LifeScan, USA).

Quantitative real-time PCR

Total RNA was extracted from tissue samples using Trizol reagent (Ambion, USA, 15596-018) and reverse transcribed to cDNA using a reverse transcription kit (Takara, Japan, RR036A), according to the manufacturers' instructions. Quantitative real-time PCR (qRT-PCR) was performed on a Quant Studio Dx Real-Time thermal cycler (Thermo Fisher, USA) with SYBR qPCR Master Mix (Vazyme, USA, Q711), and the primers listed in the Supplemental Experimental Materials. The expression of each gene was normalized to that of *Gapdh*.

Western blotting

Protein samples were prepared and western blotting was performed as described previously [19]. Briefly, liver tissues were lysed with RIPA buffer (Biocolor BioScience, China, R0095) containing a Protease and Phosphatase Inhibitor Cocktail (Thermo Fisher, USA, 78444). Protein concentrations were determined using a BCA protein assay kit (Thermo Fisher, USA, 23225). Samples containing 15 μg of total protein were separated by 10% SDS-PAGE and transferred to PVDF membranes (Merck Millipore, USA, IPVH00010). The membranes were blocked with 10% bovine serum albumin (BSA; Gibco, USA, 10099-141) in Tris-buffered saline containing Tween (EpiZyme, USA, PS103) and then incubated with primary antibodies to IRAK1 (Cell Signaling Technology, USA, 4504S) and GAPDH (Kangcheng, China, KC-5G5). Proteins of interest were visualized using Immobilon Western Chemiluminescent HRP Substrate (Merck Millipore, USA, WBKLS0500).

Statistical analysis

Results are reported as mean±standard error of the mean (SEM). The error bars in the graphs represent SEM. Differences between 2 groups were compared by 2-tailed unpaired t tests, whereas differences among 3 or more groups were compared by 1-way ANOVA with post-hoc LSD tests. Differences were considered significant if p values were less than 0.05.

Results

Construction of conventional *Irak1* knockout mice

To investigate whether *Irak1* plays significant roles in hepatosteatosis, genetic *Irak1* knockout (KO) mice were generated with CRISPR/Cas9 technology (Figure 1A). The efficiency of *Irak1* KO was confirmed at both the mRNA and protein levels (Figure 1B, 1C). The expression levels of *Irak1* mRNA in multiple organs were significantly lower in *Irak1* KO than in control mice (Figure 1B), and IRAK1 protein was undetectable in liver tissue of *Irak1* KO mice (Figure 1C). Expression of mRNAs encoding downstream inflammatory cytokines was lower in the livers of *Irak1* KO mice, with *Tnfα* and *Il1β* mRNAs being significantly lower (Figure 1D). In contrast, the levels of mRNAs encoding the main components of *Iraks* and the *Irak1*-associated pathway were similar in *Irak1* KO and control mice, except that *Irak3* mRNA was reduced in *Irak1* KO mice (Figure 1E).

Construction of NASH mouse models

To explore the effects of *Irak1* expression in NASH, experimental NASH was induced in *Irak1* KO and control mice by chronic treatment with CCl_4 or feeding MCDD. As expected, the livers of CCl_4-treated and MCDD-fed control mice were badly injured. The liver surfaces of CCl_4-treated mice were rough (Supplementary Figure 1A), whereas the livers of MCDD-fed mice were grayish-yellow in color and reduced in size (Supplementary Figure 1B). Liver weight was increased in CCl_4-treated mice (Supplementary Figure 1C), but reduced in MCDD-fed mice (Supplementary Figure 1D). Serum ALT and AST concentrations were notably elevated in both NASH models (Figure 2A, 2B), whereas H&E staining showed that clusters of lymphocytes and neutrophils were more dispersed in the livers of CCl_4-treated than of vehicle-treated mice (Supplementary Figure 2A). Massive steatosis and ballooned hepatocytes, together with inflammatory foci, were observed in hepatic sections of MCDD-fed mice (Supplementary Figure 2B). The levels of *Tnfα*, *Tgfb1*, and *Adgre1* mRNAs were increased in both NASH models, whereas *Il6* mRNA was elevated only in CCl_4-treated mice (Figure 2C, 2D). In addition, the numbers of cells positive for the immunocyte marker CD45 and for the macrophage marker F4/80 in liver tissues were increased in both NASH models (Supplementary Figure 2A–2D).

Sirius red and Masson's staining showed that treatment with CCl_4 or MCDD induced fibrogenic changes in the liver (Figure 2E–2H). The levels of expression of the fibrosis-associated genes *Sma*, *Col1a1*, *Col1a2*, and *Timp1* in the liver were enhanced by CCl_4 treatment, whereas only *Timp1* mRNA was greatly increased in MCDD-fed mice (Figure 2I, 2J). Taken together, these findings indicate that NASH mouse models had been successfully established.

Indexed in: [Current Contents/Clinical Medicine] [SCI Expanded] [ISI Alerting System] [ISI Journals Master List] [Index Medicus/MEDLINE] [EMBASE/Excerpta Medica] [Chemical Abstracts/CAS]

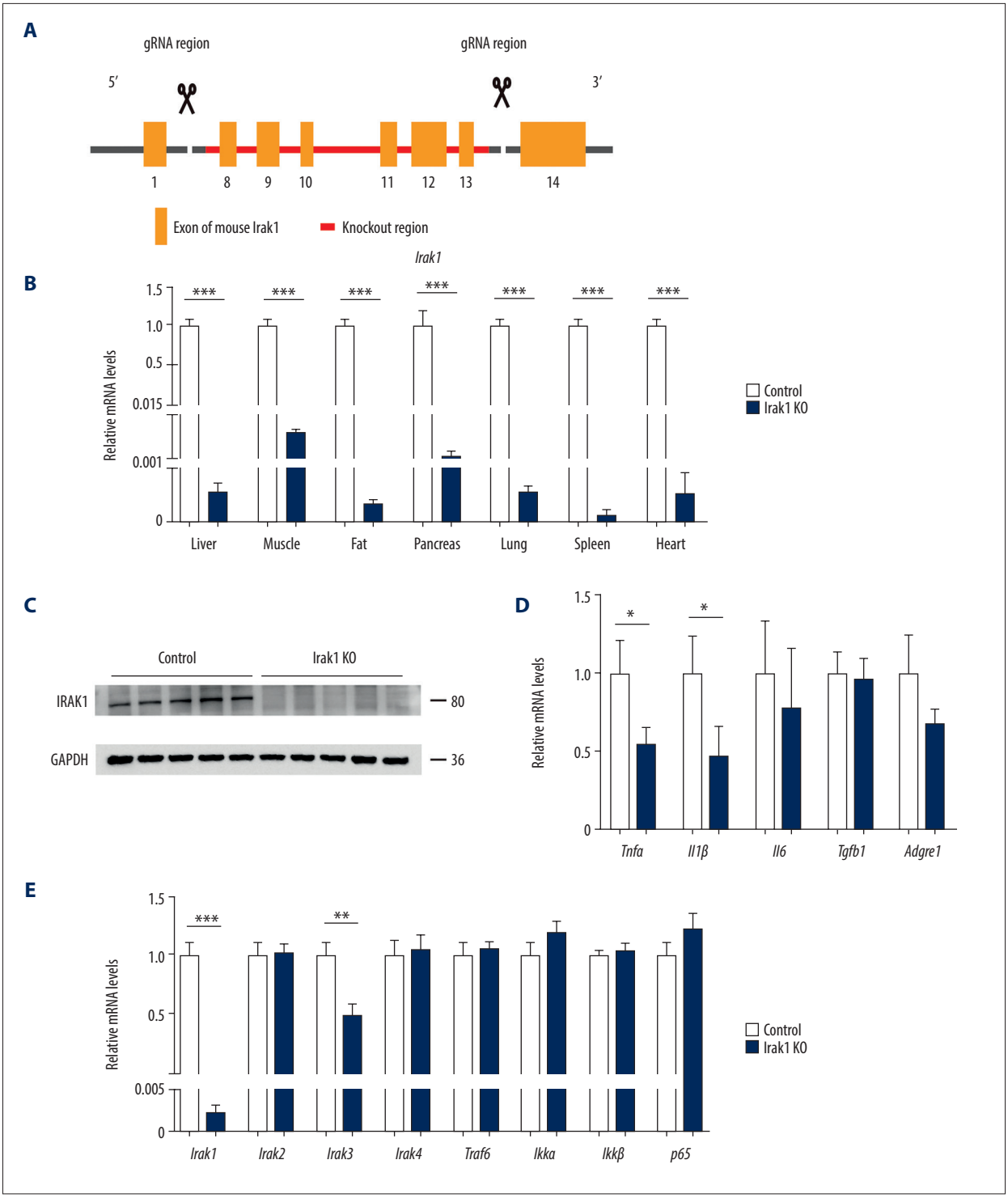

Figure 1. Generation of *Irak1* KO mice. (**A**) Schematic representation of the generation of *Irak1* KO mice. (**B**) Levels of *Irak1* mRNA in various tissues of *Irak1* KO and control mice (n=6 each). (**C**) Levels of IRAK1 protein in the livers of *Irak1* KO and control mice (n=5 each). (**D**) Hepatic levels of *Tnfα*, *Il1β*, Il6, *Tgfb1*, and *Adgre1* mRNAs in *Irak1* KO and control mice (n=6 each). (**E**) Hepatic levels of *Irak1*, *Irak2*, *Irak3*, *Irak4*, *Traf6*, *Ikkα*, *Ikkβ*, and *p65* mRNAs in *Irak1* KO and control mice (n=6 each). Data represent mean±SEM. * p<0.05, ** p<0.01, *** p< 0.001, by t tests.

Indexed in: [Current Contents/Clinical Medicine] [SCI Expanded] [ISI Alerting System] [ISI Journals Master List] [Index Medicus/MEDLINE] [EMBASE/Excerpta Medica] [Chemical Abstracts/CAS]

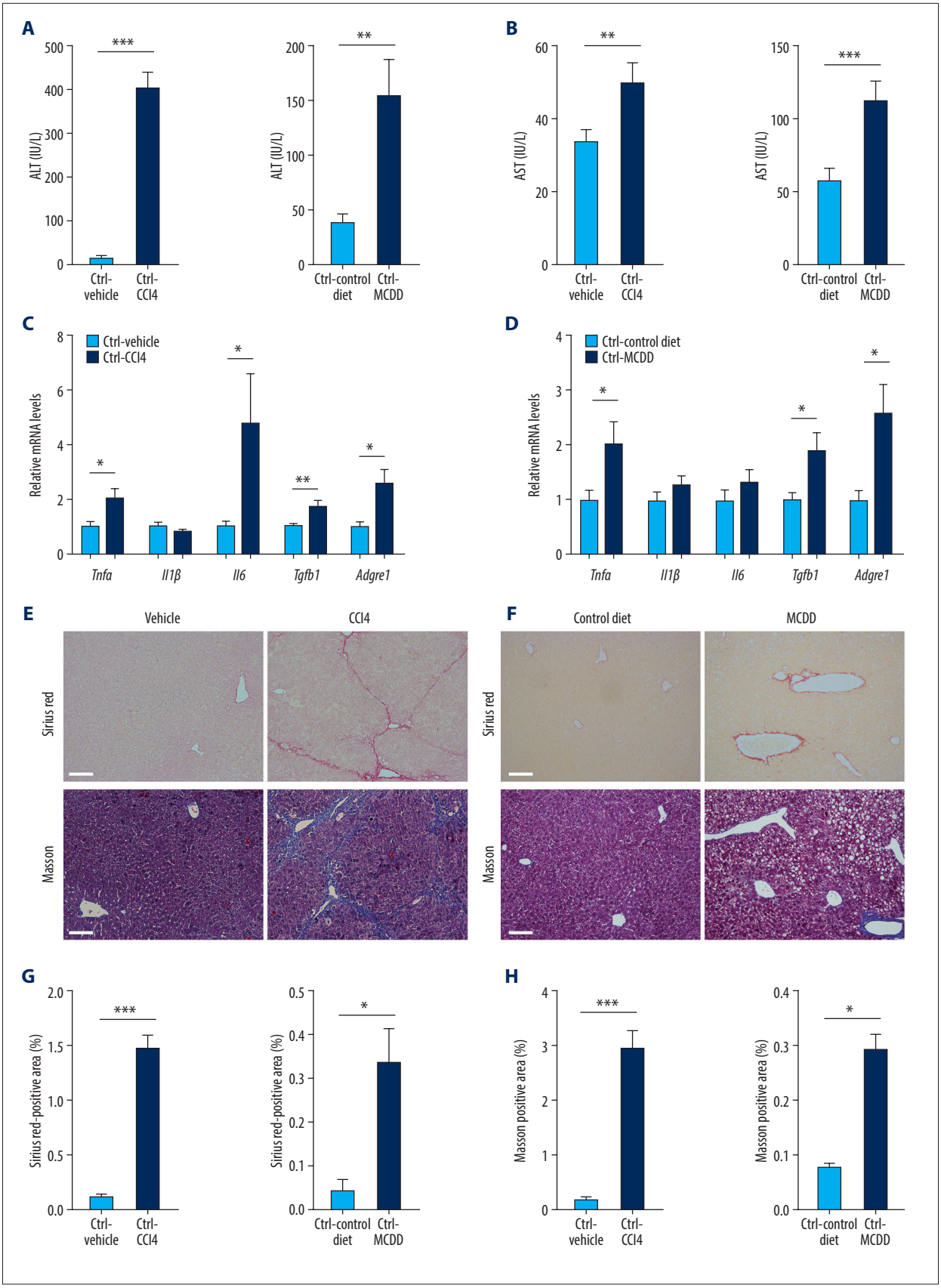

Indexed in: [Current Contents/Clinical Medicine] [SCI Expanded] [ISI Alerting System] [ISI Journals Master List] [Index Medicus/MEDLINE] [EMBASE/Excerpta Medica] [Chemical Abstracts/CAS]

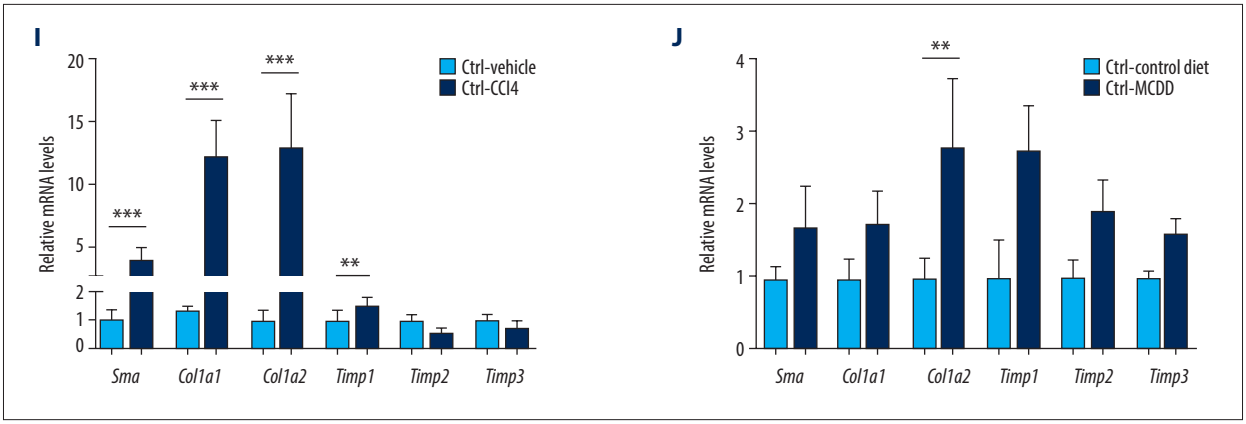

Figure 2. Generation of NASH in mice. (**A, B**) Serum (**A**) ALT and (**B**) AST levels of control mice treated for 8 weeks with CCl_4 or vehicle (n=4–6) or fed MCDD or a control diet for 6 weeks (n=5). (**C, D**) Hepatic Tnfα, *Il1*β, Il6, *Tgfb1*, and Adgre1 mRNA levels in control mice (**C**) treated for 8 weeks with CCl_4 or vehicle (n=4–6) or (**D**) fed MCDD or a control diet for 6 weeks (n=5). (**E, F**)4Representative images of Sirius red (**upper part**) and Masson staining (**bottom part**) of hepatic tissues of control mice (**E**) treated for 8 weeks with CCl_4 or vehicle (n=4–6) or (**F**) fed MCDD or a control diet for 6 weeks (n=3–4). Scale bars, 100 µm. (**G, H**) Digital quantification of (**G**) Sirius red-positive and (**H**) Masson stain-positive areas in control mice treated for 8 weeks with CCl_4 or vehicle (n=4–6) or fed MCDD or a control diet for 6 weeks (n=3–4). (**I, J**) Hepatic *Sma*, *Col1a1*, *Col1a2*, *Timp1*, *Timp2*, and *Timp3* mRNA levels in control mice (**I**) treated for 8 weeks with CCl_4 or vehicle (n=4–6) or (**J**) fed MCDD or a control diet for 6 weeks (n=5). Data represent mean±SEM. * p<0.05, ** p<0.01, *** p< 0.001, by t test.

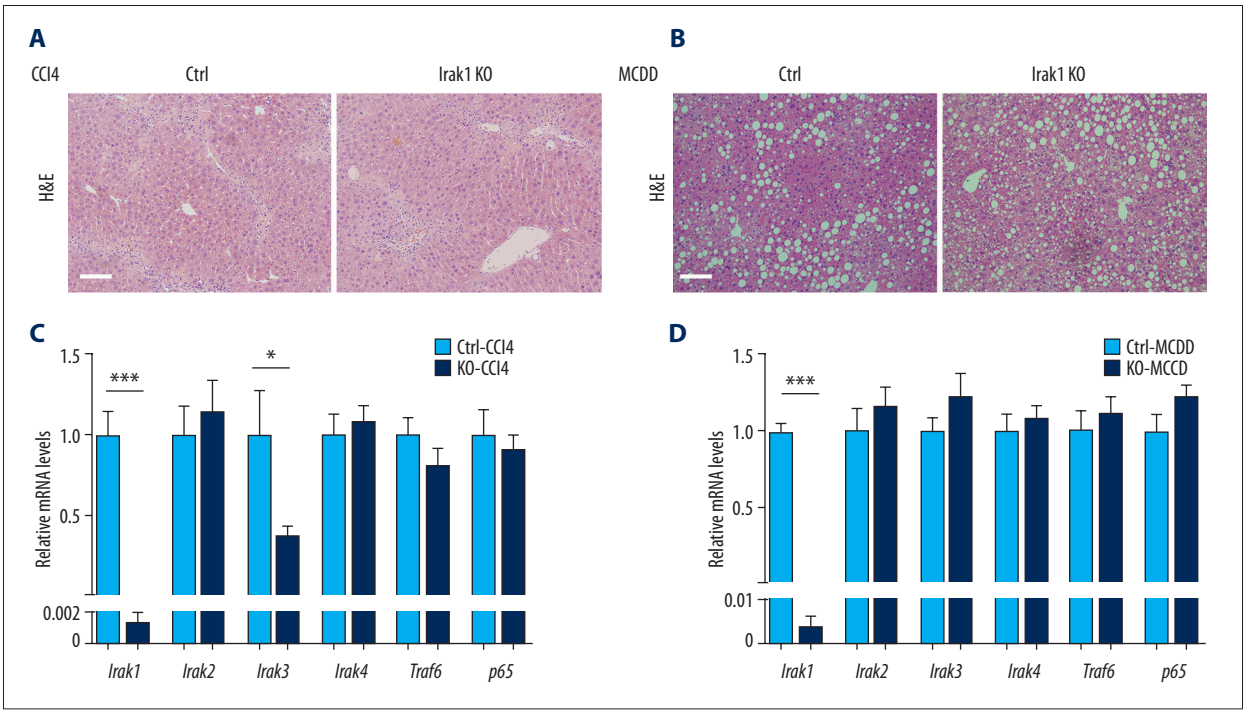

Indexed in: [Current Contents/Clinical Medicine] [SCI Expanded] [ISI Alerting System] [ISI Journals Master List] [Index Medicus/MEDLINE] [EMBASE/Excerpta Medica] [Chemical Abstracts/CAS]

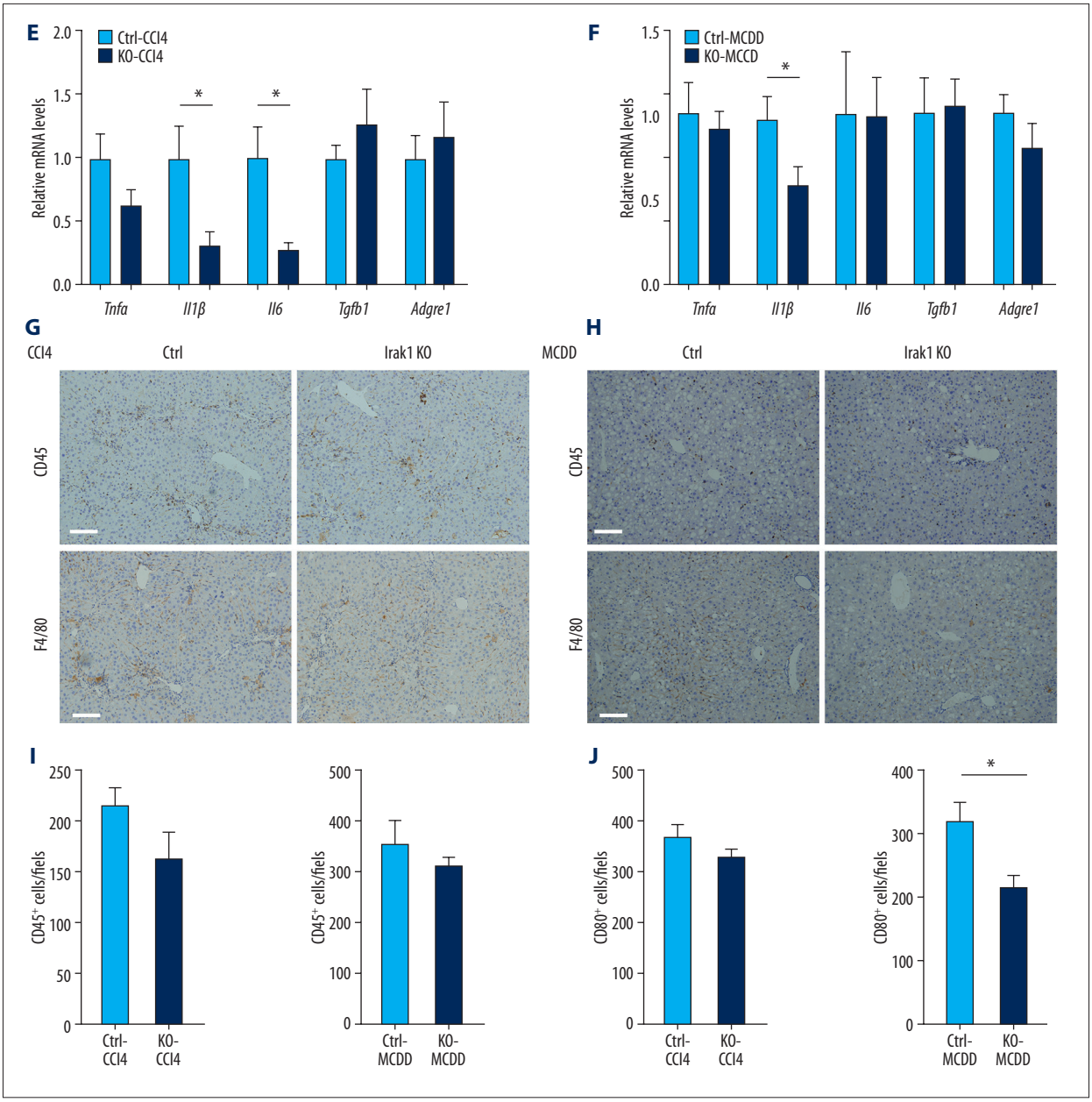

Figure 3. Effects of *Irak1* KO on key pro-inflammatory factors and inflammatory cell infiltration in the livers in mouse models of NASH. (**A, B**) Representative H&E-stained liver sections of *Irak1* KO and control mice following (**A**) treatment with CCl_4 for 8 weeks or (**B**) MCDD feeding for 6 weeks. Scale bars, 100 μm. (**C, D**) Hepatic *Irak1*, *Irak2*, *Irak3*, *Irak4*, *Traf6*, and *p65* mRNA levels in *Irak1* KO and control mice following (**C**) treatment with CCl_4 for 8 weeks (n=5) or (**D**) MCDD feeding for 6 weeks (n=5–6). (**E, F**) Hepatic Tnfα, *Il1*β, *Il6*, *Tgfb1*, and *Adgre1* mRNA levels in *Irak1* KO and control mice following (**E**) treatment with CCl_4 for 8 weeks (n=5) or (**F**) MCDD feeding for 6 weeks (n=5–6). (**G, H**) Representative CD45 (**upper part**) and F4/80 (**bottom part**) positively-stained liver sections of *Irak1* KO and control mice following (**G**) treatment with CCl_4 for 8 weeks or (**H**) MCDD feeding for 6 weeks. Scale bars, 100 μm. (**I, J**) Numbers of (**I**) CD45-positive and (**J**) F4/80-positive cells per field from *Irak1* KO and control mice following CCl_4 treatment for 8 weeks (n=3–4, 5 fields per mouse) or MCDD feeding for 6 weeks (n=3–4, 5 fields per mouse). Data represent mean±SEM. * p<0.05, ** p<0.01, *** p<0.001, by t test.

Indexed in: [Current Contents/Clinical Medicine] [SCI Expanded] [ISI Alerting System] [ISI Journals Master List] [Index Medicus/MEDLINE] [EMBASE/Excerpta Medica] [Chemical Abstracts/CAS]

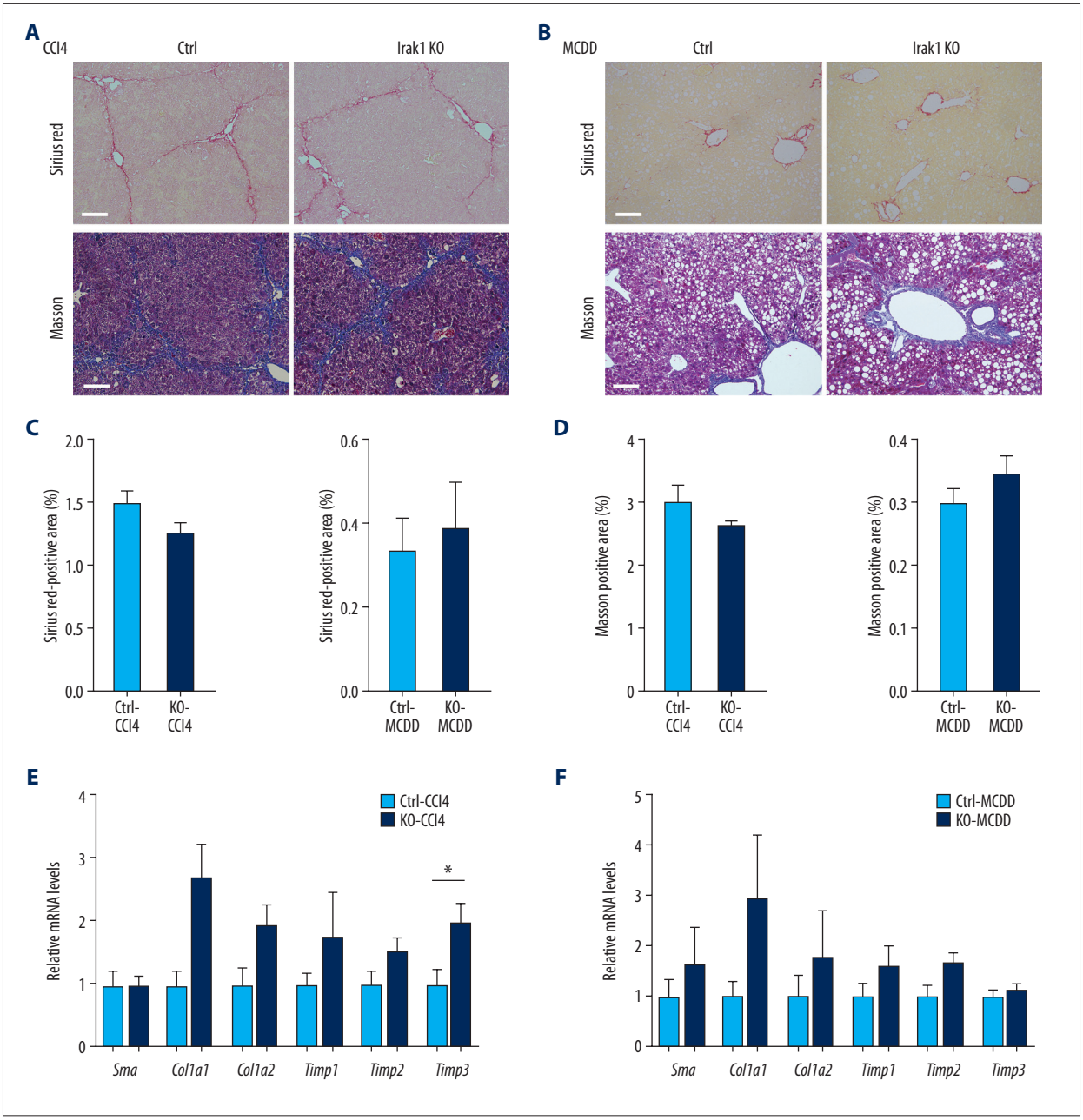

Figure 4. Effects of *Irak1* KO on collagen deposition in mouse models of NASH. (**A, B**) Representative Sirius red (**upper part**) and Masson (**bottom part**) stained liver sections of *Irak1* KO and control mice following (**A**) CCl_4 treatment for 8 weeks (n=5–6) or (**B**) MCDD feeding for 6 weeks (n=3–4). Scale bars, 100 µm. (**C, D**) Digital quantification of (**C**) Sirius red-positive and (**D**) Masson stain-positive areas of livers of *Irak1* KO and control mice following CCl_4 treatment for 8 weeks (n=5–6) or MCDD feeding for 6 weeks (n=3–4). (**E, F**) Hepatic levels of *Sma*, *Col1a1*, *Col1a2*, *Timp1*, *Timp2*, and *Timp3* mRNAs in *Irak1* KO and control mice following (**E**) CCl_4 treatment for 8 weeks (n=5–6) or (**F**) MCDD feeding for 6 weeks (n=5). Data represent mean±SEM. * $p<0.05$ by t test.

Indexed in: [Current Contents/Clinical Medicine] [SCI Expanded] [ISI Alerting System] [ISI Journals Master List] [Index Medicus/MEDLINE] [EMBASE/Excerpta Medica] [Chemical Abstracts/CAS]

Irak1 ablation mildly ameliorated inflammatory cell infiltration

To determine the role of *Irak1* in hepatic steatosis, *Irak1* KO and control mice were challenged with CCl_4 or MCDD. Liver morphology did not differ in *Irak1* KO and control mice treated with CCl_4 or fed MCDD (Supplementary Figure 3A, 3B). Although treatment with CCl_4 or MCDD enhanced serum ALT and AST concentrations, there were no differences between *Irak1* KO and control mice (Supplementary Figure 4A, 4B). H&E staining of liver sections of both NASH models showed no differences between *Irak1* KO and control mice (Figure 3A, 3B). Liver expression of the main components of *Iraks* and the *Irak1*-associated pathway did not differ in *Irak1* KO and control mice, except that the expression of *Irak3* mRNA was markedly lower in *Irak1* KO mice after treatment with CCl_4 (Figure 3C, 3D).

To determine whether *Irak1* KO affects levels of inflammation in mice challenged with CCl_4 or MCDD, the expression of mRNAs encoding downstream inflammatory cytokines was determined. The expression of *Il1*β mRNA was markedly lower in the livers of *Irak1* KO than of control mice treated with CCl_4 or MCDD (Figure 3E, 3F), whereas the expression of *Il6* mRNA was significantly lower in *Irak1* KO than in control mice treated with CCl_4, but not with MCDD (Figure 3E). The numbers of cells positive for the immunocyte marker CD45 were similar in *Irak1* KO and control mice after treatment with CCl_4 or MCDD, whereas the number of cells positive for the macrophage marker F4/80 was lower in *Irak1* KO than in control mice only after treatment with MCDD (Figure 3G–3J). Taken together, these findings showed that *Irak1* deletion had a mildly ameliorative effect on inflammatory cell infiltration in mouse models of NASH.

Irak1 knockout did not attenuate liver fibrosis

To determine whether loss of *Irak1* affected liver injury and fibrogenesis, hepatic collagen deposition was analyzed in *Irak1* KO and control mice. Although Sirius red and Masson staining showed marked deposition of collagen in livers following the administration of CCl_4 or MCDD (Figure 2E, 2F), collagen deposition was comparable in *Irak1* KO and control mice (Figure 4A–4D). The hepatic levels of mRNAs encoding profibrogenic genes in *Irak1* KO mice were unchanged by treatment with CCl_4 or MCDD, except that *Timp3* mRNA level was lower in *Irak1* KO mice treated with CCl_4 (Figure 4E, 4F). These findings showed that *Irak1* deficiency did not affect hepatic collagen deposition.

Irak1 knockout did not affect lipid and glucose metabolism

Analysis of lipid metabolism showed that, compared with vehicle-treated mice, CCl_4-treated mice had markedly elevated serum TG and TC levels, but there were no differences between *Irak1* KO and control mice (Supplementary Figure 4C). Similarly, serum and hepatic TG levels were comparable in *Irak1* KO and control mice, despite hepatic TG being greatly increased in mice treated with MCDD (Supplementary Figure 4D). Furthermore, lipid metabolism signaling factors were not altered in *Irak1* KO and control mice treated with CCl_4 or MCDD (Supplementary Figure 4E, 4F). Intraperitoneal glucose tolerance tests (IPGTT) and insulin tolerance tests (ITT) showed no differences between *Irak1* KO and control mice treated with CCl_4 or vehicle, indicating that *Irak1* KO had no effect on serum glucose concentrations (Supplementary Figure 5A, 5B).

Discussion

In the liver, most injuries damage epithelial cells (hepatocytes and/or cholangiocytes), leading to the release of inflammatory mediators and the initiation of an anti-fibrinolytic cascade [4,5]. Lipopolysaccharide (LPS)/TLR4 signaling activation is essential for the activation of hepatic stellate cells and liver-resident macrophages [20]. Inhibition of the IRAK1-related TLR/IL1R pathway may attenuate hepatic fibrogenesis. For example, the microRNA miR-146a-5p has been found to downregulate the levels of expression of IRAK1 and TRAF6 during liver fibrosis, followed by modulation of the IRAK4/IRAK1/TRAF6 axis [15–17]. In addition, miR-146a-5p was shown to modulate hepatic fibrosis through Smad4/TGFβ [16,21]. Pacritinib, an inhibitor of IRAK1, JAK2, FLT3, and CSF1R, showed antifibrotic effects in a mouse model of liver fibrosis [18]. However, miR-146a-5p and pacritinib are multi-target modulators that cannot assess the therapeutic effects of IRAK1 on fibrogenesis. Thus, despite these findings on IRAK1-related pathways, the effects of *Irak1* itself on liver fibrosis had not been investigated in *Irak1*-specific KO mice.

Our study showed that *Irak1* KO in the liver could reduce the expression of mRNAs encoding inflammatory cytokines, like *Il1*β, with and without CCl_4 or MCDD treatment. A study of polymicrobial sepsis showed that TLR4-dependent *Il6* and *Il1*β mRNAs were down-regulated in *Irak1* KO mice, whereas TLR2-dependent responses were unaffected [13]. Reduced oxidative tissue damage during endotoxemia, due to decreases in inflammatory responses, was also observed in *Irak1* KO mice [22]. IRAK1 deficiency in HCC could attenuate IL1β/IRAK1 inflammatory signaling and further diminish HCC progression [14]. These findings, showing that inflammation was attenuated in *Irak1* KO mice, were consistent with our results. However, we found that infiltrating lymphocytes were not significantly reduced in *Irak1* KO mice when challenged with CCl_4 or MCDD.

TGF-β1 is a multifunctional cytokine that regulates inflammatory cell infiltration, cell growth, differentiation, and fibrosis [23].

Indexed in: [Current Contents/Clinical Medicine] [SCI Expanded] [ISI Alerting System] [ISI Journals Master List] [Index Medicus/MEDLINE] [EMBASE/Excerpta Medica] [Chemical Abstracts/CAS]

TGF-β1 is considered a key mediator in fibrotic diseases [24–26]. Consistent with previous findings, our study found that the levels of *Tgfb1* mRNA were increased in both NASH models, but were unaffected by *Irak1* KO. The lack of effect of *Irak1* KO on fibrosis progression may be due to the constitutive expression of *Tgfb1*.

We also analyzed the expression of the main components of *Iraks* and their associated pathways, including *Irak1*, Irak2, *Irak3*, and Irak4. Hepatic *Irak3*, which is abundant in liver tissue and negatively regulates TLR signaling [27,28], was reduced in *Irak1* KO mice. Irak2 and *Irak3* were able to partially complement the ability of *Irak1* to activate NF-κB [29,30], suggesting that Irak2 and *Irak3* may compensate for the effects of *Irak1* KO on liver fibrosis in these mouse models of NASH.

Conclusions

The present study, which tested the effects of *Irak1* KO on liver inflammation and fibrogenesis in mouse models of NASH, showed that *Irak1* KO reduced the expression of hepatic inflammatory genes, such as *Il1*β. *Irak1* KO did not ameliorate fibrogenesis in mice with liver injury induced by CCl_4 or MCDD. The compensatory effects of Irak2, *Irak3*, and other components might maintain lymphocyte infiltration, resulting in the constitutive expression of *Tgfb1* mRNA, with no effect on liver fibrosis. microRNAs and inhibitors with multiple targets may affect fibrosis through more complicated pathways than *Irak1* alone.

Supplementary Data

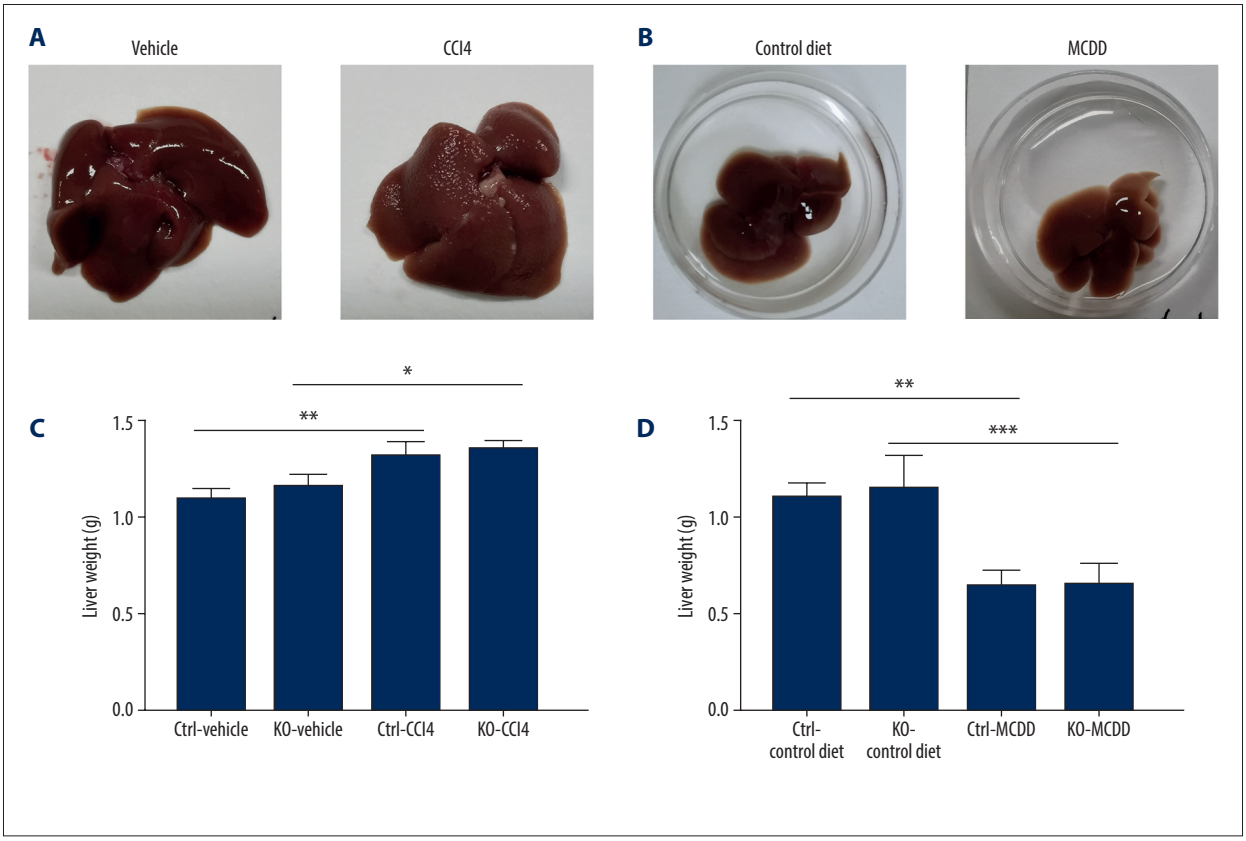

Supplementary Figure 1. Gross morphology and weight of livers. (**A, B**) Representative images of the livers of control mice (**A**) treated with CCl_4 or vehicle for 8 weeks or (**B**) fed MCDD or a control diet for 6 weeks. (**C, D**) Liver weights of *Irak1* KO and control mice (**C**) treated with CCl_4 or vehicle for 8 weeks (n=4–6) or (**D**) fed MCDD or a control diet for 6 weeks (n=5). Data represent mean±SEM. * $p<0.05$, ** $p<0.01$, *** $p<0.001$, by 1-way ANOVA with post-hoc LSD test.

Indexed in: [Current Contents/Clinical Medicine] [SCI Expanded] [ISI Alerting System] [ISI Journals Master List] [Index Medicus/MEDLINE] [EMBASE/Excerpta Medica] [Chemical Abstracts/CAS]

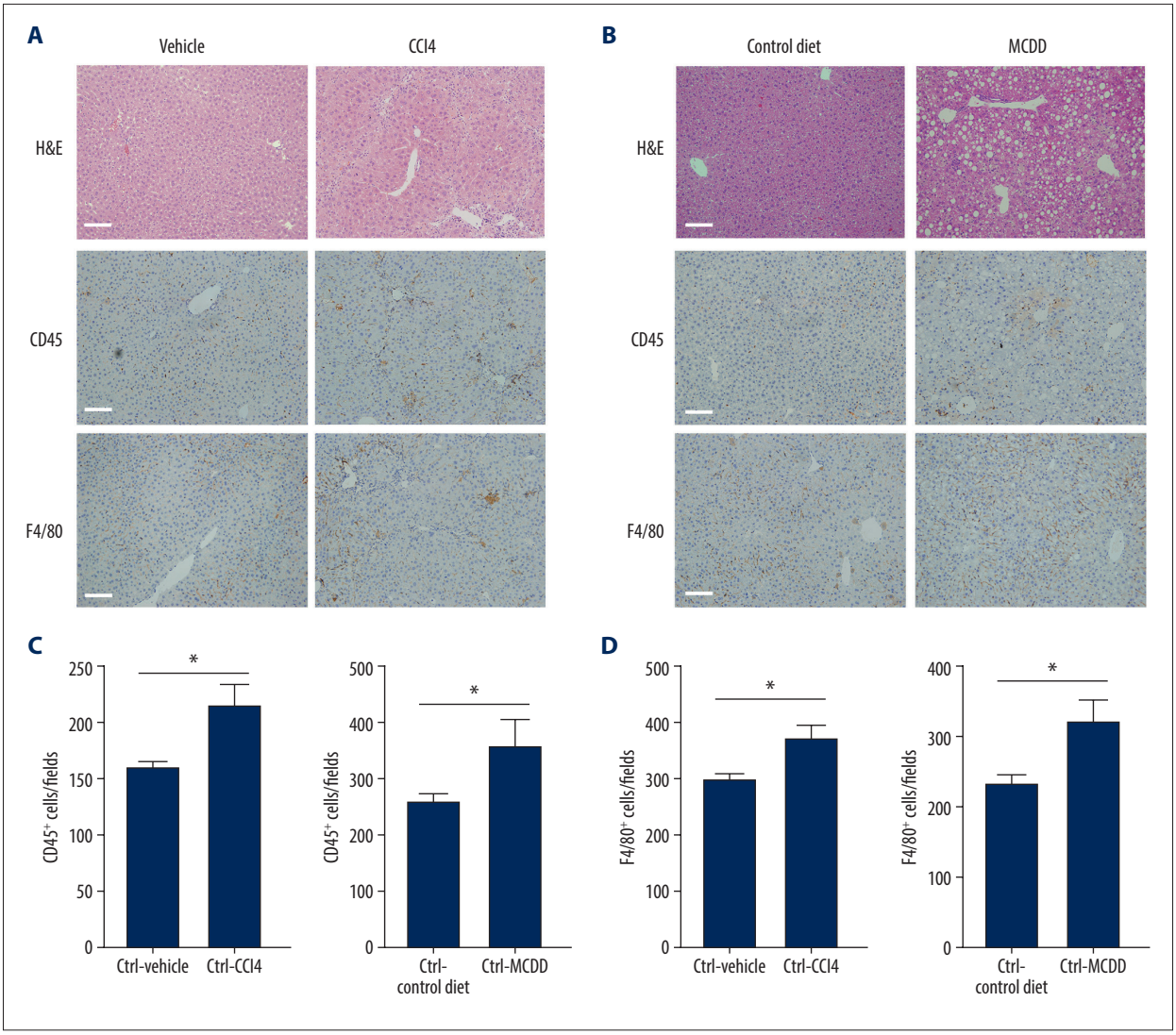

Supplementary Figure 2. Analysis of key pro-inflammatory factors and numbers of immunocytes and macrophages. (**A, B**) Representative images of H&E- (**upper part**), CD45- (**middle part**) and F4/80- (**bottom part**) stained liver sections of control mice (**A**) treated with CCl_4 or vehicle for 8 weeks or (**B**) fed MCDD or a control diet for 6 weeks. Scale bars, 100 µm. (**C, D**) Numbers of (**C**) CD45-positive and (**D**) F4/80-positive cells per field in liver sections of control mice treated with CCl_4 or vehicle for 8 weeks (n=3–4, 5 fields per mouse) or fed MCDD or a control diet for 6 weeks (n=3–4, 5 fields per mouse). Data represent mean±SEM. * $p<0.05$ by t test.

Indexed in: [Current Contents/Clinical Medicine] [SCI Expanded] [ISI Alerting System] [ISI Journals Master List] [Index Medicus/MEDLINE] [EMBASE/Excerpta Medica] [Chemical Abstracts/CAS]

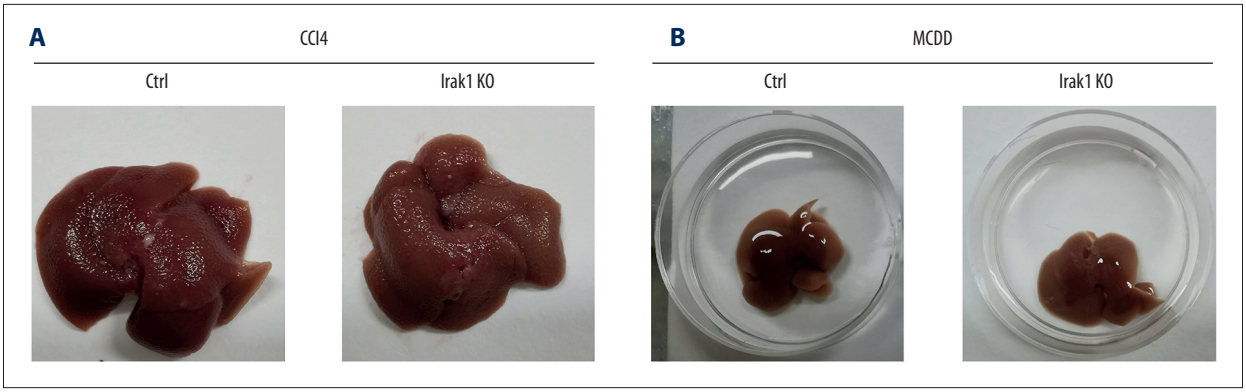

Supplementary Figure 3. Gross hepatic morphology of mice treated with CCl_4 or MCDD. (**A, B**) Representative hepatic images of *Irak1* KO and control mice following (**A**) CCl_4 treatment for 8 weeks or (**B**) MCDD feeding for 6 weeks.

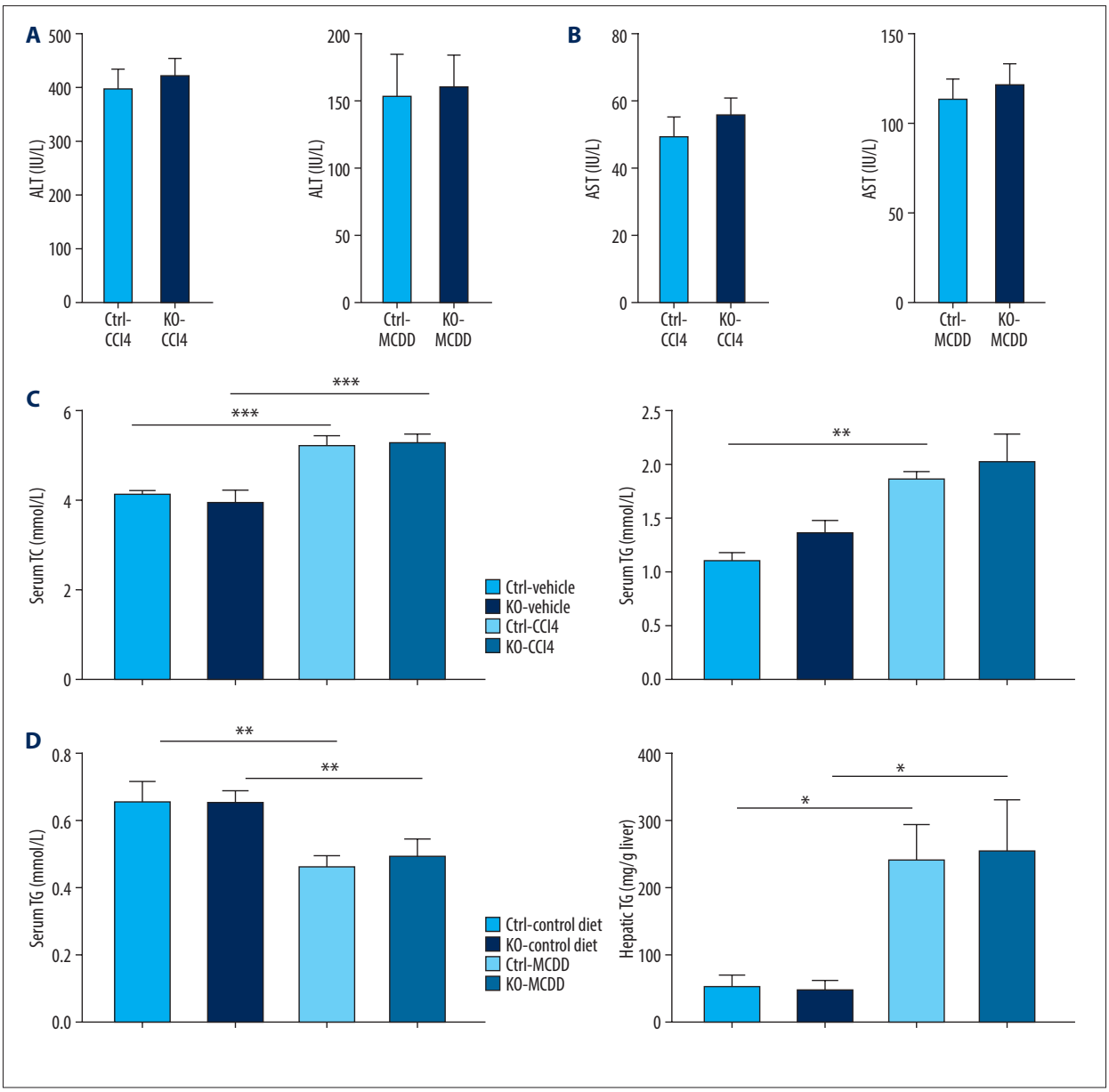

Indexed in: [Current Contents/Clinical Medicine] [SCI Expanded] [ISI Alerting System] [ISI Journals Master List] [Index Medicus/MEDLINE] [EMBASE/Excerpta Medica] [Chemical Abstracts/CAS]

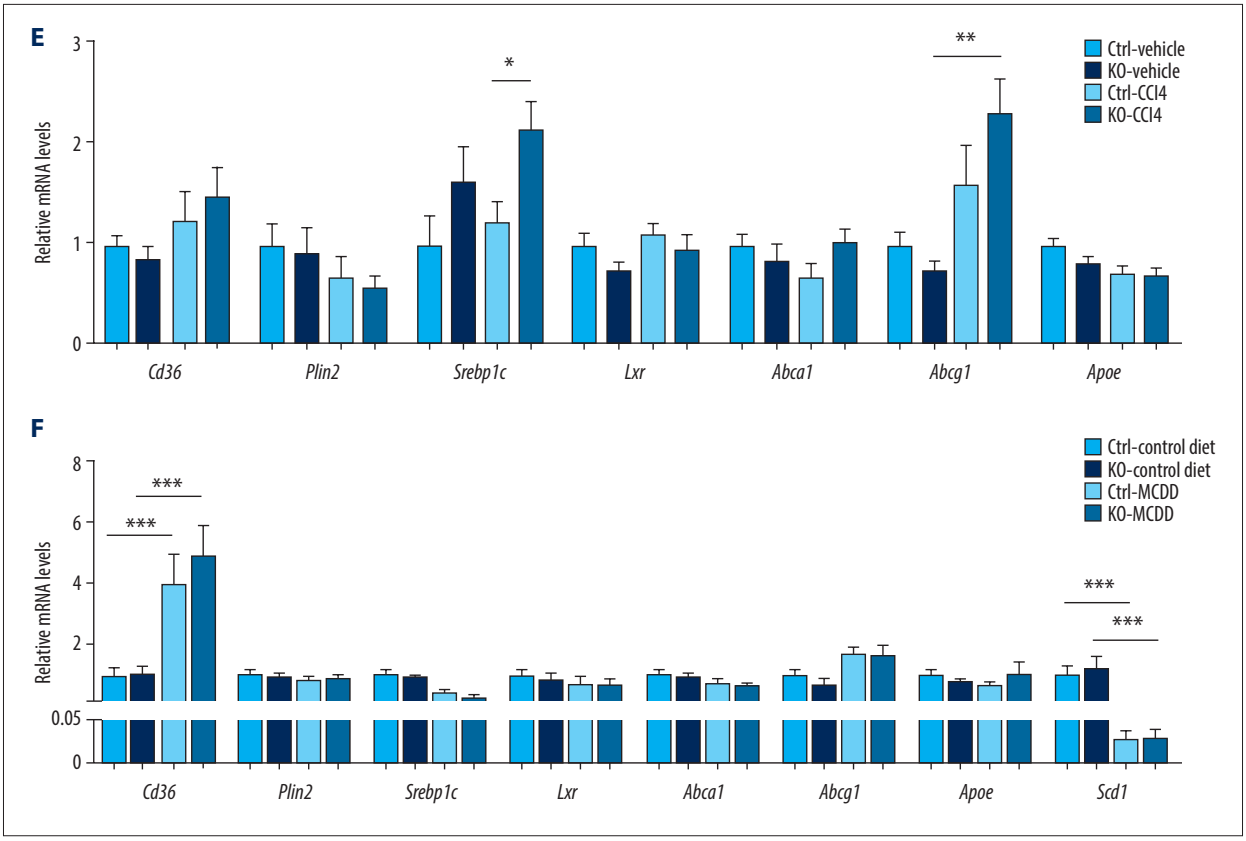

Supplementary Figure 4. Lipid metabolism and metabolic signaling factors in the CCl_4 and MCDD models. (**A, B**) Serum concentrations of (**A**) ALT and (**B**) AST of control mice following CCl_4 treatment for 8 weeks (n=5–6) or MCDD feeding for 6 weeks (n=5). (**C**) Serum TC and TG concentrations of *Irak1* KO and control mice following CCl_4 or vehicle treatment for 8 weeks (n=4–6). (**D**) Serum and hepatic TG concentrations of *Irak1* KO and control mice following MCDD or control diet feeding for 6 weeks (n=5). (**E, F**) Hepatic levels of *Cd36*, *Plin2*, *Srebp1c*, *Lxr*, *Abca1*, *Abcg1*, *Apoe* (and *Scd1*) mRNAs in *Irak1* KO and control mice (**E**) treated with CCl_4 or vehicle for 8 weeks (n=4–6) or (**F**) fed MCDD or a control diet for 6 weeks (n=8–10). Data represent mean±SEM. * $p<0.05$, ** $p<0.01$, *** $p<0.001$, by t test (2 groups) or 1-way ANOVA with post-hoc LSD test (more than 2 groups)

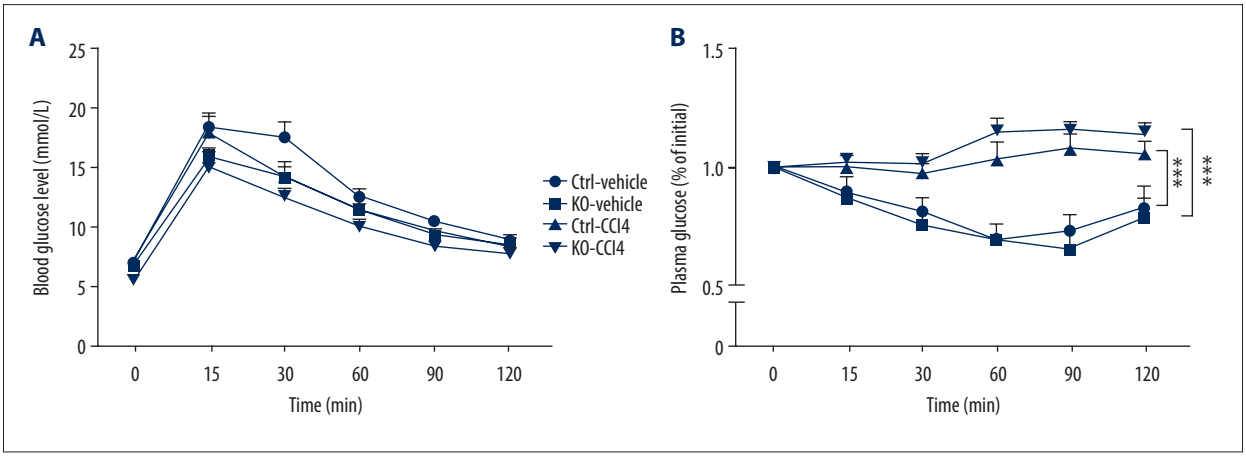

Supplementary Figure 5. Effect of *Irak1* KO on glucose metabolism in the CCl_4 model. (**A**) Glucose tolerance tests of *Irak1* KO and control mice treated with CCl_4 or vehicle for 6 weeks (n=4–6). (**B**) Insulin tolerance test of *Irak1* KO and control mice treated with CCl_4 or vehicle for 7 weeks (n=4–6). Data represent mean±SEM. * $p<0.05$, ** $p<0.01$, *** $p<0.001$, by 1-way ANOVA with post-hoc LSD test.

Indexed in: [Current Contents/Clinical Medicine] [SCI Expanded] [ISI Alerting System] [ISI Journals Master List] [Index Medicus/MEDLINE] [EMBASE/Excerpta Medica] [Chemical Abstracts/CAS]

References:

1. Angulo P, Kleiner DE, Dam-Larsen S et al: Liver fibrosis, but no other histologic features, is associated with long-term outcomes of patients with nonalcoholic fatty liver disease. Gastroenterology, 2015; 149(2): 389–97
2. Ekstedt M, Hagström H, Nasr P et al: Fibrosis stage is the strongest predictor for disease-specific mortality in NAFLD after up to 33 years of follow-up. Hepatology, 2015; 61(5): 1547–54
3. Brunt EM, Kleiner DE, Wilson LA et al: Improvements in histologic features and diagnosis associated with improvement in fibrosis in nonalcoholic steatohepatitis: Results from the Nonalcoholic Steatohepatitis Clinical Research Network administration trials. Hepatology, 2019; 70(2): 522–31
4. Koyama Y, Brenner DA: Liver inflammation and fibrosis. J Clin Invest, 2017; 127(1): 55–64
5. Schuster S, Cabrera D, Arrese M, Feldstein AE: Triggering and resolution of inflammation in NASH. Nat Rev Gastroenterol Hepatol, 2010; 15(6): 349–64
6. Akira S, Takeda K: Toll-like receptor signalling. Nat Rev Immunol, 2004; 4(7): 499–511
7. Kesar V, Odin JA: Toll-like receptors and liver disease. Liver Int, 2014; 34(2): 184–96
8. Pradere JP, Troeger JS, Dapito DH et al: Toll-like receptor 4 and hepatic fibrogenesis. Semin Liver Dis, 2010; 30(3): 232–44
9. O'Neill L: The Toll/interleukin-1 receptor domain: A molecular switch for inflammation and host defence. Biochem Soc Trans, 2000; 28(5): 557–63
10. Janssens S, Beyaert R: Functional diversity and regulation of different interleukin-1 receptor-associated kinase (IRAK) family members. Mol Cell, 2003; 11(2): 293–302
11. Vidya MK, Kumar VG, Sejian V et al: Toll-like receptors: Significance, ligands, signaling pathways, and functions in mammals. Int Rev Immunol, 2018; 37(1): 20–36
12. Seki E, De Minicis S, Osterreicher CH et al: TLR4 enhances TGF-beta signaling and hepatic fibrosis. Nat Med, 2007; 13(11): 1324–32
13. Chandra R, Federici S, Bishwas T et al: IRAK1-dependent signaling mediates mortality in polymicrobial sepsis. Inflammation, 2013; 36(6): 1503–12
14. Su B, Luo T, Zhu J et al: Interleukin-1β/Iinterleukin-1 receptor- associated kinase 1 inflammatory signaling contributes to persistent Gankyrin activation during hepatocarcinogenesis. Hepatology, 2015; 61(2): 585–97
15. Chen Y, Zeng Z, Shen X et al: MicroRNA-146a-5p negatively regulates pro-inflammatory cytokine secretion and cell activation in lipopolysaccharide stimulated human hepatic stellate cells through Inhibition of Toll-like receptor 4 signaling pathways. Int J Mol Sci, 2016; 17(7): 1076
16. Zou Y, Cai Y, Lu D et al: MicroRNA-146a-5p attenuates liver fibrosis by suppressing profibrogenic effects of TGFβ1 and lipopolysaccharide. Cell Signal, 2017; 39: 1–8
17. Chen Y, Wu Z, Yuan B et al: MicroRNA-146a-5p attenuates irradiation-induced and LPS-induced hepatic stellate cell activation and hepatocyte apoptosis through inhibition of TLR4 pathway. Cell Death Dis, 2018; 9(2): 22
18. Al-Fayoumi S, Hashiguchi T, Shirakata Y et al: Pilot study of the antifibrotic effects of the multikinase inhibitor pacritinib in a mouse model of liver fibrosis. J Exp Pharmacol, 2018; 10: 9–17
19. Cao Y, Liu R, Jiang X et al: Nuclear-cytoplasmic shuttling of menin regulates nuclear translocation of β-catenin. Mol Cell Biol, 2009; 29(20): 5477–87
20. Pimentel-Nunes P, Soares JB, Roncon-Albuquerque R Jr. et al: Toll-like receptors as therapeutic targets in gastrointestinal diseases. Expert Opin Ther Targets, 2010; 14(4): 347–68
21. Zou Y, Li S, Li Z et al: MiR-146a attenuates liver fibrosis by inhibiting transforming growth factor-β1 mediated epithelial-mesenchymal transition in hepatocytes. Cell Signal, 2019; 58: 1–8
22. Singh N, Li L: Reduced oxidative tissue damage during endotoxemia in IRAK-1 deficient mice. Mol Immunol, 2012; 50(4): 244–52
23. Ayabe H, Anada T, Kamoya T et al: Optimal hypoxia regulates human iPSC-derived liver bud differentiation through intercellular TGFB signaling. Stem Cell Rep, 2018; 11(2): 306–16
24. Mack M, Yanagita M: Origin of myofibroblasts and cellular events triggering fibrosis. Kidney Int, 2015; 87(2): 297–307
25. Kane CJ, Hebda PA, Mansbridge JN, Hanawalt PC: Direct evidence for spatial and temporal regulation of transforming growth factor beta 1 expression during cutaneous wound healing. J Cell Physiol, 1991; 148(1): 157–73
26. Ueha S, Shand FH, Matsushima K: Cellular and molecular mechanisms of chronic inflammation-associated organ fibrosis. Front Immunol, 2012; 3: 71
27. Kobayashi K, Hernandez LD, Galán JE et al: IRAK-M is a negative regulator of Toll-like receptor signaling. Cell, 2002; 110(2): 191–202
28. Flannery S, Bowie AG: The interleukin-1 receptor-associated kinases: Critical regulators of innate immune signalling. Biochem Pharmacol, 2010; 80(12): 1981–91
29. Wesche H, Gao X, Li X et al: IRAK-M is a novel member of the Pelle/interleukin-1 receptor-associated kinase (IRAK) family. J Biol Chem, 1999; 274(27): 19403–10
30. Knop J, Martin MU: Effects of IL-1 receptor-associated kinase (IRAK) expression on IL-1 signaling are independent of its kinase activity. FEBS Lett, 1999; 448(1): 81–85

Indexed in: [Current Contents/Clinical Medicine] [SCI Expanded] [ISI Alerting System] [ISI Journals Master List] [Index Medicus/MEDLINE] [EMBASE/Excerpta Medica] [Chemical Abstracts/CAS]